

# Dualities and Topological Classification of the $S = 1$ Pyrochlore Spin Ice

Sena Watanabe\* and Yukitoshi Motome†

*Department of Applied Physics, The University of Tokyo, Tokyo 113-8656, Japan*

Haruki Watanabe‡

*Department of Physics, Hong Kong University of Science and Technology, Clear Water Bay, Hong Kong, China  
Institute for Advanced Study, Hong Kong University of Science and Technology, Clear Water Bay, Hong Kong, China*

*Center for Theoretical Condensed Matter Physics,*

*Hong Kong University of Science and Technology, Clear Water Bay, Hong Kong, China and  
Department of Applied Physics, The University of Tokyo, Tokyo 113-8656, Japan*

(Dated: March 18, 2026)

We resolve the phase diagram of the  $S = 1$  pyrochlore spin ice, which exhibits trivial paramagnetic, U(1) Coulomb, and spin nematic phases. In the monopole-free limit, the system can be effectively mapped onto 3D  $XY$  and Ising loop-gas models depending on the spin anisotropy, which provides theoretical estimates for the phase boundaries, while a macroscopic flux vector classifies the topological sectors via geometric parity rules. At finite temperatures, thermal monopoles act as a symmetry-breaking field in both 3D  $XY$  and Ising loop-gas pictures, rounding the phase transitions into continuous crossovers. These theoretical findings are corroborated by classical Monte Carlo simulations.

*Introduction.*— Highly frustrated magnets host exotic states of matter defying conventional symmetry-breaking paradigms [1–4]. A quintessential example is the classical spin-1/2 spin ice on the pyrochlore lattice [5–11], where geometrical frustration enforces the “two-in, two-out” ice rule on each tetrahedron. This local constraint can be coarse-grained into a divergence-free magnetic flux,  $\nabla \cdot \mathbf{B} = 0$ , yielding in the low-temperature limit an emergent U(1) gauge theory with an effective Maxwell action [9, 12, 13]. This emergent electromagnetism dictates the Coulomb phase, exhibiting algebraic dipolar correlations in real space and pinch-point singularities in momentum space [10, 11, 14, 15] despite the absence of conventional magnetic order. At finite temperatures, however, thermally excited magnetic monopoles [16, 17] violate the ice rule and act as a mobile magnetic plasma, whose Debye screening suppresses the dipolar correlations and degrades the Coulomb phase into a conventional paramagnet [18, 19].

While the spin-1/2 spin ice is well understood, releasing the rigid spin-length constraint opens a frontier for emergent phenomena, including magnetic moment fragmentation [20, 21], fractionalized spin liquids [22], and exotic spin nematics [23, 24]. Very recently, Pandey and Damle investigated a spin-1 extension of the pyrochlore antiferromagnetic Ising model [25], building on related developments in bipartite dimer-loop models [26, 27]. In this model, the spins can additionally occupy a nonmagnetic  $S^z = 0$  state, whose relative statistical weight is controlled by a fugacity parameter  $w$  determined by the single-ion anisotropy. Through large-scale Monte Carlo (MC) simulations, they unveiled a phase diagram characterized by three distinct regimes: a trivial paramagnetic phase for  $w < w_{c_1}$ , a  $\mathbb{Z}_2$  deconfined Coulomb phase [i.e., a full U(1) Coulomb phase] for  $w_{c_1} < w < w_{c_2}$ , and a  $\mathbb{Z}_2$  confined Coulomb phase (a spin nematic state) for

$w > w_{c_2}$ . Based on finite-size scaling analyses, Pandey and Damle suggested that the transitions at  $w_{c_1}$  and  $w_{c_2}$  belong to the 3D  $XY$  and 3D Ising universality classes, respectively [25]. The nature of such topological phases and confinement transitions has long been a central theme in condensed matter physics and lattice gauge theories [28–31], with implications extending even to water ice [32], hydrogen-bonded ferroelectrics [33], and phononic band insulators [34]. However, a unified theoretical framework capable of clarifying the microscopic origins of these universality classes—and their ultimate fate at finite temperatures—has been lacking.

In this Letter, we provide a theoretical description of this phase diagram by developing a dual formulation rooted in the principles of statistical mechanics [35]. Specifically, we establish mappings of the  $S = 1$  model onto standard statistical mechanics models defined on the dual diamond lattice. In the small- $w$  regime, the system maps onto a classical 3D  $XY$  model, demonstrating that the transition at  $w_{c_1}$  belongs to the 3D  $XY$  universality class. In the large- $w$  regime, the geometric proliferation of  $S^z = 0$  defects is described by a closed loop-gas representation that is isomorphic to the high-temperature expansion of the classical 3D Ising model, establishing the 3D Ising nature of the transition at  $w_{c_2}$ . Furthermore, we treat finite-temperature effects, showing that the thermal excitation of monopoles explicitly breaks the emergent continuous symmetry in the small- $w$  regime and acts as a topological severing of defect strings in the large- $w$  regime, thereby rounding the phase transitions into continuous crossovers.

*Model.*— We consider a classical spin-1 model of the Blume-Capel type [36, 37] on the pyrochlore lattice. Its sites reside at the midpoints of the nearest-neighbor links  $\ell = \langle \mathbf{r}_A, \mathbf{r}_B \rangle$  of the underlying bipartite diamond lattice. The local positive  $z$ -axis for each spin  $S_\ell^z \in \{-1, 0, 1\}$

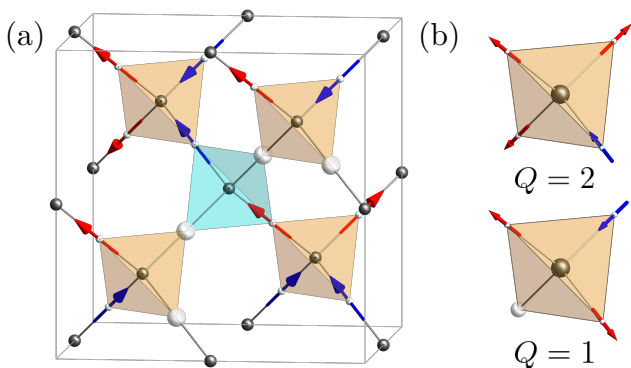


FIG. 1. (a) Geometric correspondence between the diamond and pyrochlore lattices. Black spheres represent the diamond sites, which are located at the centers of the cyan and orange tetrahedra formed by the pyrochlore sites. Arrows on the pyrochlore sites denote the spin-1 variables aligned with the local  $z$ -axis. Red and blue arrows represent  $S_\ell^z = 1$  and  $S_\ell^z = -1$ , respectively, while white spheres correspond to  $S_\ell^z = 0$ . The illustrated spin configuration satisfies the ice rule. (b) Monopole charges and their corresponding spin configurations. Odd monopole charges can exist in the spin-1 model.

points from  $\mathbf{r}_A$  to  $\mathbf{r}_B$ . This geometry is illustrated in Fig. 1. The system consists of  $L^3$  cubic unit cells, each of linear size 1, subject to periodic boundary conditions. Each unit cell contains 8 diamond-lattice sites and 16 pyrochlore sites, totaling  $N := 8L^3$  diamond-lattice sites and  $2N$  spins.

The Hamiltonian  $H := J \sum_{\langle \ell, \ell' \rangle} S_\ell^z S_{\ell'}^z + \Delta \sum_{\ell} (S_\ell^z)^2$ , comprising a nearest-neighbor exchange  $J$  and a singleton anisotropy  $\Delta := J + \mu$ , can be recast into a perfect-square

$$H = \frac{J}{2} \sum_{\mathbf{r}} \left( \sum_{\ell \in \mathbf{r}} S_\ell^z \right)^2 + \mu \sum_{\ell} (S_\ell^z)^2, \quad (1)$$

where  $\ell \in \mathbf{r}$  denotes the four links connected to the diamond-lattice site  $\mathbf{r}$ . Magnetic monopoles are characterized by the discrete divergence of the spin configuration, which is defined for sublattices A and B as  $\nabla \cdot \mathbf{S}_{\mathbf{r}_A} := \sum_{\ell \in \mathbf{r}_A} S_\ell^z$  and  $\nabla \cdot \mathbf{S}_{\mathbf{r}_B} := -\sum_{\ell \in \mathbf{r}_B} S_\ell^z$ , respectively.

Introducing the fugacities  $w := e^{-\mu/T}$  and  $v := e^{-J/(2T)}$ , the partition function  $Z := \sum_{\{S_\ell^z\}} e^{-H/T}$  is rewritten as

$$Z = \sum_{\{Q_{\mathbf{r}}\}} \sum_{\{S_\ell^z\}} \left( \prod_{\mathbf{r}} \delta_{\nabla \cdot \mathbf{S}_{\mathbf{r}}, Q_{\mathbf{r}}} \right) v^{\sum_{\mathbf{r}} Q_{\mathbf{r}}^2} w^{\sum_{\ell} (S_\ell^z)^2}. \quad (2)$$

For  $J \gg T$  ( $v \ll 1$ ), thermal monopoles are suppressed, and states satisfying the ice rule  $Q_{\mathbf{r}} = 0$  dominate.

*Duality Mapping to the XY Model.*— To describe the small- $w$  regime, we perform a duality transformation in the monopole-free limit ( $v = 0$ ), building on the

well-known mapping of divergence-free current models onto the XY model [38, 39]. Gauss's law constraint  $\nabla \cdot \mathbf{S}_{\mathbf{r}} = 0$  is enforced by introducing a continuous phase field  $\theta_{\mathbf{r}} \in [0, 2\pi)$  via the Fourier integral  $\delta_{\nabla \cdot \mathbf{S}_{\mathbf{r}}, 0} = \int_0^{2\pi} \frac{d\theta_{\mathbf{r}}}{2\pi} e^{-i\theta_{\mathbf{r}} \nabla \cdot \mathbf{S}_{\mathbf{r}}}$ . By inserting this into the partition function and performing a discrete integration by parts on the lattice,  $\sum_{\mathbf{r}} \theta_{\mathbf{r}} \nabla \cdot \mathbf{S}_{\mathbf{r}} = -\sum_{\ell=\langle \mathbf{r}_A, \mathbf{r}_B \rangle} (\theta_{\mathbf{r}_B} - \theta_{\mathbf{r}_A}) S_\ell^z$ , we find that the partition function factorizes over links:

$$Z_{v=0} = \int \mathcal{D}\theta \prod_{\langle \mathbf{r}, \mathbf{r}' \rangle} [1 + 2w \cos(\theta_{\mathbf{r}} - \theta_{\mathbf{r}'})], \quad (3)$$

where  $\mathcal{D}\theta := \prod_{\mathbf{r}} \frac{d\theta_{\mathbf{r}}}{2\pi}$ . For sufficiently small  $w$ , the Taylor expansion  $\ln(1 + X) \approx X$  holds, yielding

$$Z_{v=0} \approx \int \mathcal{D}\theta e^{2w \sum_{\langle \mathbf{r}, \mathbf{r}' \rangle} \cos(\theta_{\mathbf{r}} - \theta_{\mathbf{r}'})}. \quad (4)$$

This is the partition function of the classical 3D XY model defined on the diamond lattice. The emergent XY spins interact with an effective ferromagnetic coupling  $K = 2w$ . Because the higher-order harmonics neglected in the Taylor expansion correspond to irrelevant operators in the renormalization-group sense, this mapping guarantees that the continuous phase transition at  $w_{c_1}$  belongs to the 3D XY universality class, providing a theoretical foundation for the recent numerical conjecture [25]. Using the numerical estimate for the critical coupling  $K_c \approx 0.7877$  [40], we estimate the critical fugacity for the U(1) Coulomb phase onset to be  $w_{c_1} = K_c/2 \approx 0.3939$ . The deviation from the numerical result  $w_{c_1} = 0.3609(1)$  obtained by Pandey and Damle [25] may stem from the higher-order terms in the generalized XY action.

*Mapping to the Loop-Gas Model.*— The approximation used for the dual XY mapping breaks down in the large- $w$  regime. We therefore introduce a real-space “loop-gas” picture, a conceptual framework useful for understanding extended defects and confinement transitions [41, 42]. For the system of  $N$  diamond-lattice sites and  $2N$  links, the links at  $v = 0$  are predominantly occupied by  $S_\ell^z = \pm 1$  spins due to their large weight, while  $S_\ell^z = 0$  states (relative weight  $1/w$ ) act as minority defects. The ice rule dictates that these defect strings never possess endpoints and must form closed-loop configurations  $C$ . Thus, the partition function is given by

$$Z_{v=0} = w^{2N} W(\emptyset) \sum_C \frac{W(C)}{W(\emptyset)} \left( \frac{1}{w} \right)^{|C|}, \quad (5)$$

where  $W(C)$  is the number of valid background spin configurations for a fixed closed-loop configuration  $C$ .

We evaluate this ratio using Pauling's approximation. Assuming that all  $2N$  links can freely take  $S_\ell^z = \pm 1$ , the number of loop-free vacuum configurations is  $W(\emptyset) \approx 2^{2N} (3/8)^N$ , where  $3/8$  is the probability of satisfying

the ice rule at each of the  $N$  sites. For a configuration  $C$  consisting of  $|C|$  links in total, these links are fixed to  $S_\ell^z = 0$ , leaving  $2N - |C|$  free links. Furthermore, assuming no loop intersections, the configuration  $C$  traverses exactly  $|C|$  sites. Thus, the system contains  $N - |C|$  loop-free sites and  $|C|$  loop-traversed sites. At the loop-free sites, the probability of satisfying the ice rule remains  $3/8$ . Conversely, at the loop-traversed sites, two of the four connecting links are fixed to zero, increasing the probability that the remaining two free links sum to zero to  $\binom{2}{1}/2^2 = 1/2$ . Thus, the number of valid configurations compatible with  $C$  is  $W(C) \approx 2^{2N-|C|} (3/8)^{N-|C|} (1/2)^{|C|}$ . Taking the ratio to the vacuum weight yields the configurational entropy reduction factor  $W(C)/W(\emptyset) \approx 2^{-|C|} (3/8)^{N-|C|} (1/2)^{|C|} = (2/3)^{|C|}$ . This gives

$$Z_{v=0} \approx w^{2N} W(\emptyset) \sum_C \left( \frac{2}{3w} \right)^{|C|}. \quad (6)$$

This loop gas is isomorphic to the high-temperature expansion of the zero-field 3D Ising model. In terms of Ising spins  $\sigma_{\mathbf{r}} \in \{-1, 1\}$ , the partition function  $Z_{\text{Ising}} = \sum_{\{\sigma_{\mathbf{r}}\}} \exp\left(K \sum_{\langle \mathbf{r}, \mathbf{r}' \rangle} \sigma_{\mathbf{r}} \sigma_{\mathbf{r}'}\right)$  can be expanded as

$$Z_{\text{Ising}} = (\cosh K)^{2N} 2^N \sum_C x^{|C|}, \quad (7)$$

where  $x := \tanh K$ . The proliferation transition of the loop gas, marking the onset of the U(1) Coulomb phase, maps onto the ferromagnetic transition of this Ising model [43]. While the bare weight  $x \approx 2/(3w)$  relies on Pauling's approximation, which neglects short-range spatial correlations such as loop self-intersections, these geometric corrections correspond to irrelevant local perturbations that merely renormalize the effective fugacity without altering the universality class. This isomorphism establishes that the topological confinement transition at  $w_{c_2}$  falls into the 3D Ising universality class, explaining the critical exponents observed numerically [25]. Consequently, equating the theoretical estimate with the critical point  $K_c \approx 0.3698$  [44] via  $\frac{2}{3w_{c_2}} \approx \tanh K_c$ , we predict  $w_{c_2} \approx 1.884$ . The agreement with the numerical result  $1.8904(1)$  [25] demonstrates that this mapping captures the essential physics, with the deviation reflecting the higher-order corrections to Pauling's approximation.

*Topological Classification via Global Flux.* — At  $v = 0$ , the macroscopic global flux threading the system,

$$\mathbf{P} := \frac{1}{L} \sum_{\ell=\langle \mathbf{r}_A, \mathbf{r}_B \rangle} (\mathbf{r}_B - \mathbf{r}_A) S_\ell^z, \quad (8)$$

acts as a topological invariant that distinguishes the three phases. Since the vertical displacement along any link is  $|z_B - z_A| = 1/4$ , the system can be partitioned by  $4L$  horizontal planes. Let  $C_k$  be the set of links intersecting

the  $k$ -th plane. The net flux  $W_z^{(k)}$  crossing this plane is given by

$$W_z^{(k)} = \sum_{\ell \in C_k} \text{sgn}(z_B - z_A) S_\ell^z. \quad (9)$$

The ice rule ensures that this flux is conserved across any plane ( $W_z^{(k)} = W_z$ ), yielding  $P_z = W_z \in \mathbb{Z}$ . By cubic symmetry,  $\mathbf{P} \in \mathbb{Z}^3$ .

The parity of  $P_z$  can be evaluated modulo 2. The total number of links crossing a plane is  $4L^2$ . Since  $S_\ell^z \equiv (S_\ell^z)^2 \pmod{2}$  and the geometric sign satisfies  $\text{sgn}(z_B - z_A) \equiv 1 \pmod{2}$ , we find  $P_z \equiv \sum_{\ell \in C_k} (S_\ell^z)^2 \pmod{2}$ . If we let  $n_0$  be the number of  $S_\ell^z = 0$  defect links intersecting the plane, the sum counts the number of nonzero links; thus, the remaining  $4L^2 - n_0$  links must have  $(S_\ell^z)^2 = 1$ . Since  $4L^2$  is an even integer, we obtain the congruence relation:

$$P_z \equiv 4L^2 - n_0 \equiv n_0 \pmod{2}. \quad (10)$$

Thus, the parity of the global flux is tied to the parity of  $n_0$ . This geometric property dictates the macroscopic topological sectors. In the trivial phase ( $w < w_{c_1}$ ), directed  $S_\ell^z = \pm 1$  closed loops are dilute and cannot wrap around the periodic boundaries, freezing the macroscopic flux to  $\mathbf{P} = \mathbf{0}$ . In the U(1) Coulomb phase ( $w_{c_1} < w < w_{c_2}$ ), both directed  $S_\ell^z = \pm 1$  loops and undirected  $S_\ell^z = 0$  strings proliferate. The macroscopic  $S_\ell^z = 0$  strings can cross a plane an odd number of times [ $n_0 \equiv 1 \pmod{2}$ ], unlocking the parity constraint and permitting all integer flux sectors ( $\mathbf{P} \in \mathbb{Z}^3$ ). Finally, in the spin nematic phase ( $w > w_{c_2}$ ), the  $S_\ell^z = 0$  strings cease to proliferate. Finite closed loops must traverse a plane an even number of times, enforcing  $n_0 \equiv 0 \pmod{2}$ . This parity constraint eliminates odd flux sectors [ $\mathbf{P} \in (2\mathbb{Z})^3$ ], encapsulating the  $\mathbb{Z}_2$  flux-confined Coulomb phase where macroscopic  $S^z = 0$  strings are confined and only the  $S^z = \pm 1$  loops proliferate. This parity-based topological classification parallels the exact description of the 3D toric code limit using macroscopic loop parities [45]. As is evident, this topological nature relies on the absence of monopoles ( $v = 0$ ). Once finite-temperature effects are introduced, these topological distinctions become blurred.

*Finite-Temperature Effects.* — At any finite temperature  $T > 0$ , the monopole fugacity  $v$  is small but finite. By incorporating the leading effect of  $0 < v \ll 1$  and repeating the XY mapping in the small- $w$  regime, we find that the partition function becomes [46]

$$Z \approx \int \mathcal{D}\theta \exp \left( 2w \sum_{\langle \mathbf{r}, \mathbf{r}' \rangle} \cos(\theta_{\mathbf{r}} - \theta_{\mathbf{r}'}) + 2v \sum_{\mathbf{r}} \cos \theta_{\mathbf{r}} \right). \quad (11)$$

Physically, thermal monopoles introduce a sine-Gordon term acting as a uniform external magnetic field. This field explicitly breaks the continuous U(1) symmetry of

the dual  $XY$  model, rounding the phase transition into a continuous crossover.

An analogous conclusion emerges in the large- $w$  loop-gas representation. Incorporating thermal monopoles allows strings to possess endpoints. The loop-gas partition function is generalized to a sum over general graphs  $G$ ,

$$Z \approx w^{2N} W(\emptyset) \sum_G \left(\frac{2}{3w}\right)^{|G|} (\sqrt{3}v)^{|\partial G|}, \quad (12)$$

where  $|G|$  is the number of links in the graph, and  $|\partial G|$  denotes the total number of endpoints. This matches the high-temperature expansion of the 3D Ising model in a uniform magnetic field  $h$ , defined as  $Z_{\text{Ising}} = \sum_{\{\sigma_r\}} \exp\left(K \sum_{\langle r, r' \rangle} \sigma_r \sigma_{r'} + h \sum_r \sigma_r\right)$ . As detailed in the Supplemental Material [46], this yields

$$Z_{\text{Ising}} = (\cosh K)^{2N} (\cosh h)^N 2^N \sum_G x^{|G|} y^{|\partial G|}, \quad (13)$$

with the effective parameters identified as  $x := 2/(3w)$  and  $y := \sqrt{3}v$ . Since a uniform magnetic field eliminates the phase transition in the effective Ising model, the macroscopic topological singularity of the proliferation transition in the original model degrades into a continuous crossover due to the topological severing of strings at  $v > 0$ . We note that an analogous explicit breaking of emergent gauge symmetries by relevant perturbations has been shown to impact confinement transitions in hydrogen-bonded systems [33]. This topological fragility contrasts sharply with 3D  $\mathbb{Z}_2$  topological phases, such as the 3D toric code [45, 47] and exactly solvable Kitaev spin liquids [48, 49], where strict local constraints ensure the absence of string endpoints. In those models, the macroscopic loop parity (or Wilson loop) remains a robust topological order parameter, thereby preserving sharp finite-temperature phase transitions [45, 49].

Despite the loss of such strict thermodynamic singularities in our model, the geometric nature of the defect strings dictates a highly nontrivial scaling of the finite-temperature correlation length  $\xi$  governed by the monopole plasma. Debye screening alters the spin correlations from an algebraic to an exponential decay, with  $\xi$  scaling as  $v^{-Q^2/2}$ , where  $Q$  is the minimal deconfined monopole charge. In the U(1) Coulomb phase, tensionless defect strings deconfine the fundamental  $Q = \pm 1$  monopoles, yielding  $\xi \propto v^{-1/2}$  [18, 19]. In stark contrast, the finite tension of  $S^z = 0$  strings in the spin nematic phase topologically confines the  $Q = \pm 1$  monopoles. Instead, double monopoles with  $Q = \pm 2$ , connected by tensionless spin-flip Dirac strings, emerge as the leading free plasma, resulting in a drastically enhanced correlation length  $\xi \propto v^{-2}$ . Because  $v = e^{-J/(2T)}$ , this exceptionally long  $\xi$  at low temperatures ( $J \gtrsim T$ ) can easily exceed accessible system sizes, rendering the exponential screening practically unobservable. This physical mechanism effectively preserves the algebraic correlations on

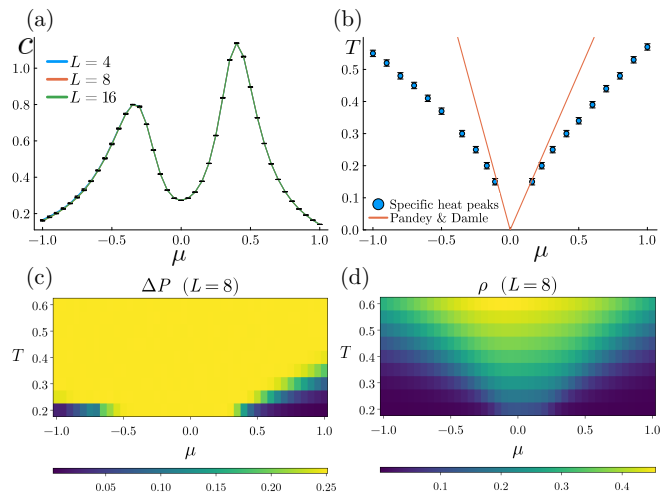


FIG. 2. Results of MC simulations. (a) System-size dependence of the specific heat at  $T = 0.3$ . (b) Peak positions of the specific heat for  $L = 4$  and the phase boundaries determined numerically in the monopole-free limit by Pandey and Damle [25]. Heat maps of (c) the deviation  $\Delta P$  and (d) the monopole density  $\rho$  for  $L = 8$ . Panels (c) and (d) indicate that the presence of thermal monopoles causes the macroscopic flux to deviate from integer values.

finite length scales, rigorously justifying the monopole-free approximation and the apparent criticality reported by Pandey and Damle [25].

*Monte Carlo Simulations.*— To verify our predictions, we perform classical MC simulations fixing  $J = 1$ . A standard MC sweep comprises  $2N$  single-spin heat-bath updates. Measurements are typically taken over  $5 \times 10^6$  sweeps after  $10^6$  thermalization sweeps. In the highly frustrated regime (small  $\Delta$ ), we accelerate relaxation using a hybrid scheme combining heat-bath updates with the short-loop algorithm [50, 51] ( $10^5$  thermalization,  $5 \times 10^5$  measurement sweeps). We calculate the specific heat per diamond-lattice site,  $c := -\frac{T}{N} \frac{\partial^2 F}{\partial T^2} = \frac{1}{N} \frac{\langle E^2 \rangle - \langle E \rangle^2}{T^2}$ , where  $E$  is the total energy. We also compute the macroscopic global flux  $\mathbf{P}$  and the monopole density,  $\rho := \frac{1}{N} \langle \sum_r |\nabla \cdot \mathbf{S}_r| \rangle$ . In the presence of monopoles, the flux  $\mathbf{P}$  is not restricted to  $\mathbb{Z}^3$  or  $(2\mathbb{Z})^3$ . We define  $\Delta P := \sum_{i=x,y,z} \langle (P_i - [P_i])^2 \rangle$  to measure the deviations of  $\mathbf{P}$  from integer values, where  $[\cdot]$  denotes the nearest integer.

As the parameters are tuned across the predicted boundaries, the specific heat exhibits broad maxima. MC data for three different system sizes in Fig. 2(a) reveal that the peak height of  $c$  saturates and does not grow with increasing linear system size  $L$ . This absence of a macroscopic thermodynamic divergence provides numerical evidence that, at finite temperatures ( $v > 0$ ), the phase transitions are rounded into continuous crossovers due to the explicit symmetry breaking by thermal monopoles. The peak positions of the spe-

cific heat are plotted in Fig. 2(b). We observe that the peak positions deviate from the phase boundaries in the monopole-free limit reported by Pandey and Damle [25] as the temperature  $T$  increases (i.e., as  $v$  becomes larger). This behavior supports the conclusion that the phase transitions are smeared into crossovers.

Furthermore, the measurements of  $\mathbf{P}$  visualize the loss of topological quantization. While our  $v = 0$  theory dictates that the components of  $\mathbf{P}$  must be confined to exactly zero, all integers, or even integers depending on the phase, the finite-temperature MC data in Fig. 2(c) reveal continuous deviations from these quantized values.[52] Furthermore, Fig. 2(d) shows that this loss of quantization is directly accompanied by a finite thermal monopole density. This fractional leakage of the macroscopic winding numbers mirrors our theoretical conclusion: the thermal excitation of monopoles blurs the topological distinctions between the macroscopic phases.

*Conclusion and Outlook.* — In conclusion, dual mappings of the  $S = 1$  pyrochlore spin ice onto 3D  $XY$  and Ising loop-gas models unveil the microscopic origins of its macroscopic phases and their topological classification via geometric parity rules. Crucially, we demonstrated that thermal monopoles explicitly break the continuous  $XY$  symmetry and topologically sever defect strings, rounding the finite-temperature phase transitions into continuous crossovers, as corroborated by our MC simulations.

Looking forward, exploring quantum  $S = 1$  spin ice [53–55] promises rich exotic phenomena, where transverse and quadrupolar fluctuations might stabilize novel quantum spin liquids or supersolids. More broadly, our findings establish a conceptual paradigm for diverse frustrated systems governed by ice rules and emergent gauge fields [33, 34]. Notably, mapping the hydrogen-bond network of high-pressure water ice onto our  $S = 1$  model reveals that monopole screening eliminates the thermodynamic singularity between molecular ice-VII and non-molecular ice-X [56]. This resolves a longstanding thermodynamic paradox, highlighting a universal interplay among emergent electromagnetism, geometric string topologies, and macroscopic phase behaviors from frustrated magnetism to dense molecular networks.

We thank Naoto Nagaosa, Tibor Rakovszky, and Inti Sodemann for useful discussions. The work of S.W. is supported by JST SPRING, Grant No. JPMJSP2108. The work of Y.M. is supported by JSPS KAKENHI Grant No. JP25H01247. The work of H.W. is supported by JSPS KAKENHI Grant No. JP24K00541. The work of H.W. was conducted in part during the program “Generalised symmetries and anomalies in quantum phases of matter 2026” (code: ICTS/GSYQM2026/01).

---

\* watanabe-sena397@g.ecc.u-tokyo.ac.jp

† motome@ap.t.u-tokyo.ac.jp

‡ hwatanabe@ust.hk

- [1] L. Balents, Spin liquids in frustrated magnets, *Nature* **464**, 199 (2010).
- [2] L. Savary and L. Balents, Quantum spin liquids: a review, *Rep. Prog. Phys.* **80**, 016502 (2017).
- [3] J. Knolle and R. Moessner, A field guide to spin liquids, *Annu. Rev. Condens. Matter Phys.* **10**, 451 (2019).
- [4] C. Broholm, R. J. Cava, S. A. Kivelson, D. G. Nocera, M. R. Norman, and T. Senthil, Quantum spin liquids, *Science* **367**, eaay0668 (2020).
- [5] M. J. Harris, S. T. Bramwell, D. F. McMorrow, T. Zeiske, and K. W. Godfrey, Geometrical frustration in the ferromagnetic pyrochlore  $\text{Ho}_2\text{Ti}_2\text{O}_7$ , *Phys. Rev. Lett.* **79**, 2554 (1997).
- [6] A. P. Ramirez, A. Hayashi, R. J. Cava, R. Siddharthan, and B. S. Shastry, Zero-point entropy in ‘spin ice’, *Nature* **399**, 333 (1999).
- [7] S. T. Bramwell and M. J. P. Gingras, Spin ice state in frustrated magnetic pyrochlore materials, *Science* **294**, 1495 (2001).
- [8] M. J. P. Gingras and P. A. McClarty, Quantum spin ice: a search for gapless quantum spin liquids in pyrochlore magnets, *Rep. Prog. Phys.* **77**, 056501 (2014).
- [9] M. Hermele, M. P. A. Fisher, and L. Balents, Pyrochlore photons: The  $U(1)$  spin liquid in a  $S = 1/2$  three-dimensional frustrated magnet, *Phys. Rev. B* **69**, 064404 (2004).
- [10] S. V. Isakov, K. Gregor, R. Moessner, and S. L. Sondhi, Dipolar spin correlations in classical pyrochlore magnets, *Phys. Rev. Lett.* **93**, 167204 (2004).
- [11] C. L. Henley, Power-law spin correlations in pyrochlore antiferromagnets, *Phys. Rev. B* **71**, 014424 (2005).
- [12] D. A. Huse, W. Krauth, R. Moessner, and S. L. Sondhi, Coulomb and liquid dimer models in three dimensions, *Phys. Rev. Lett.* **91**, 167004 (2003).
- [13] R. Moessner and S. L. Sondhi, Three-dimensional resonating-valence-bond liquids and their excitations, *Phys. Rev. B* **68**, 184512 (2003).
- [14] T. Fennell, P. P. Deen, A. R. Wildes, K. Schmalzl, D. Prabhakaran, A. T. Boothroyd, R. J. Aldus, D. F. McMorrow, and S. T. Bramwell, Magnetic coulomb phase in the spin ice  $\text{Ho}_2\text{Ti}_2\text{O}_7$ , *Science* **326**, 415 (2009).
- [15] D. J. P. Morris, D. A. Tennant, S. A. Grigera, B. Klemke, C. Castelnovo, R. Moessner, C. Czarnik, M. Meissner, K. C. Rule, J.-U. Hoffmann, K. Kiefer, S. Gerischer, D. Slobinsky, and R. S. Perry, Dirac strings and magnetic monopoles in the spin ice  $\text{Dy}_2\text{Ti}_2\text{O}_7$ , *Science* **326**, 411 (2009).
- [16] C. Castelnovo, R. Moessner, and S. L. Sondhi, Magnetic monopoles in spin ice, *Nature* **451**, 42 (2008).
- [17] L. D. C. Jaubert and P. C. W. Holdsworth, Signature of magnetic monopole and dirac string dynamics in spin ice, *Nat. Phys.* **5**, 258 (2009).
- [18] I. A. Ryzhkin, Magnetic relaxation in rare-earth oxide pyrochlores, *J. Exp. Theor. Phys.* **101**, 481 (2005).
- [19] C. Castelnovo, R. Moessner, and S. L. Sondhi, Debye-Hückel theory for spin ice at low temperature, *Phys. Rev. B* **84**, 144435 (2011).
- [20] M. E. Brooks-Bartlett, S. T. Banks, L. D. C. Jaubert,

- A. Harman-Clarke, and P. C. W. Holdsworth, Magnetic-moment fragmentation and monopole crystallization, *Phys. Rev. X* **4**, 011007 (2014).
- [21] S. Petit, E. Lhotel, S. Guitteny, O. Florea, J. Robert, P. Bonville, I. Mirebeau, J. Ollivier, H. Mutka, E. Ressouche, C. Decorse, M. Ciomaga Hatnean, and G. Balakrishnan, Observation of magnetic fragmentation in spin ice, *Nat. Phys.* **12**, 746 (2016).
- [22] J. Rehn, A. Sen, and R. Moessner, Fractionalized  $\mathbb{Z}_2$  classical heisenberg spin liquids, *Phys. Rev. Lett.* **118**, 047201 (2017).
- [23] N. Shannon, K. Penc, and Y. Motome, Nematic, vector-multipole, and plateau-liquid states in the classical  $o(3)$  pyrochlore antiferromagnet with biquadratic interactions in applied magnetic field, *Phys. Rev. B* **81**, 184409 (2010).
- [24] Y. Wan and M. J. P. Gingras, Color ice states, weathervane modes, and order by disorder in the bilinear-biquadratic pyrochlore heisenberg antiferromagnet, *Phys. Rev. B* **94**, 174417 (2016).
- [25] J. Pandey and K. Damle,  $S = 1$  pyrochlore magnets with competing anisotropies: A tale of two coulomb phases,  $\mathbb{Z}_2$  flux confinement and XY-like transitions (2025), arXiv:2512.11623 [cond-mat.str-el].
- [26] S. Kundu and K. Damle, Flux fractionalization transition in anisotropic  $S = 1$  antiferromagnets and dimer-loop models, *Phys. Rev. X* **15**, 011018 (2025).
- [27] S. Kundu and K. Damle, Flux confinement-deconfinement transition of dimer-loop models on three-dimensional bipartite lattices (2025), arXiv:2510.11607.
- [28] E. Fradkin and S. H. Shenker, Phase diagrams of lattice gauge theories with higgs fields, *Phys. Rev. D* **19**, 3682 (1979).
- [29] J. B. Kogut, An introduction to lattice gauge theory and spin systems, *Rev. Mod. Phys.* **51**, 659 (1979).
- [30] T. Senthil and M. P. A. Fisher,  $\mathbb{Z}_2$  gauge theory of electron fractionalization in strongly correlated systems, *Phys. Rev. B* **62**, 7850 (2000).
- [31] A. Kitaev, Anyons in an exactly solved model and beyond, *Ann. Phys.* **321**, 2 (2006).
- [32] O. Benton, O. Sikora, and N. Shannon, Classical and quantum theories of proton disorder in hexagonal water ice, *Phys. Rev. B* **93**, 125143 (2016).
- [33] C.-H. Chern and N. Nagaosa, Gauge field and the confinement-deconfinement transition in hydrogen-bonded ferroelectrics, *Phys. Rev. Lett.* **112**, 247602 (2014).
- [34] Z. Han and S. A. Kivelson, Emergent gauge fields in band insulators, *Proc. Natl. Acad. Sci. U.S.A.* **122**, e2421778122 (2025).
- [35] F. J. Wegner, Duality in generalized ising models and phase transitions without local order parameters, *J. Math. Phys.* **12**, 2259 (1971).
- [36] M. Blume, Theory of the first-order magnetic phase change in  $\text{UO}_2$ , *Phys. Rev.* **141**, 517 (1966).
- [37] H. Capel, On the possibility of first-order phase transitions in ising systems of triplet ions with zero-field splitting, *Physica* **32**, 966 (1966).
- [38] J. V. José, L. P. Kadanoff, S. Kirkpatrick, and D. R. Nelson, Renormalization, vortices, and symmetry-breaking perturbations in the two-dimensional planar model, *Phys. Rev. B* **16**, 1217 (1977).
- [39] R. Savit, Duality in field theory and statistical systems, *Rev. Mod. Phys.* **52**, 453 (1980).
- [40] K. Hattori and H. Tsunetsugu, Classical monte carlo study for antiferro quadrupole orders in a diamond lattice, *J. Phys. Soc. Jpn.* **85**, 094001 (2016).
- [41] A. W. Sandvik and R. Moessner, Correlations and confinement in nonplanar two-dimensional dimer models, *Phys. Rev. B* **73**, 144504 (2006).
- [42] L. D. C. Jaubert, M. J. Harris, T. Fennell, R. G. Melko, S. T. Bramwell, and P. C. W. Holdsworth, Topological-sector fluctuations and curie-law crossover in spin ice, *Phys. Rev. X* **3**, 011014 (2013).
- [43] A. Nahum, J. T. Chalker, P. Serna, M. Ortuño, and A. M. Somoza, 3d loop models and the  $\text{CP}^{n-1}$  sigma model, *Phys. Rev. Lett.* **107**, 110601 (2011).
- [44] Y. Deng and H. W. J. Blöte, Simultaneous analysis of several models in the three-dimensional ising universality class, *Phys. Rev. E* **68**, 036125 (2003).
- [45] J. Nasu, T. Kaji, K. Matsuura, M. Udagawa, and Y. Motome, Phase transitions to fractionalized mott insulators in an anisotropic 3d kitaev model, *Phys. Rev. B* **89**, 115125 (2014).
- [46] See Supplemental Material for detailed derivations of the duality mapping to the XY model at finite temperatures and the mapping to the Ising model with a magnetic field.
- [47] C. Castelnovo and C. Chamon, Topological order in a three-dimensional toric code at finite temperature, *Phys. Rev. B* **78**, 155120 (2008).
- [48] I. Kimchi, J. G. Analytis, and A. Vishwanath, Three-dimensional quantum spin liquids in models of harmonic-honeycomb iridates and phase diagram in an infinite- $d$  approximation, *Phys. Rev. B* **90**, 205126 (2014).
- [49] J. Nasu, M. Udagawa, and Y. Motome, Vaporization of kitaev spin liquids, *Phys. Rev. Lett.* **113**, 197205 (2014).
- [50] G. T. Barkema and M. E. J. Newman, Monte carlo simulation of ice models, *Phys. Rev. E* **57**, 1155 (1998).
- [51] R. G. Melko, B. C. den Hertog, and M. J. P. Gingras, Long-range order at low temperatures in dipolar spin ice, *Phys. Rev. Lett.* **87**, 067203 (2001).
- [52] Note that  $\Delta P$  is a system-size-dependent quantity that approaches 1/4 in the completely random limit. We expect that, as the system approaches the thermodynamic limit,  $\Delta P$  converges to 1/4 for all values of  $\mu$  at any finite temperature.
- [53] L. Savary and L. Balents, Coulombic quantum liquids in spin-1/2 pyrochlores, *Phys. Rev. Lett.* **108**, 037202 (2012).
- [54] N. Shannon, O. Sikora, F. Pollmann, K. Penc, and P. Fulde, Quantum ice: A quantum monte carlo study, *Phys. Rev. Lett.* **108**, 067204 (2012).
- [55] O. Benton, O. Sikora, and N. Shannon, Seeing the light: Experimental signatures of emergent electromagnetism in a quantum spin ice, *Phys. Rev. B* **86**, 075154 (2012).
- [56] S. Watanabe, Y. Motome, and H. Watanabe, Continuous crossover between high-pressure ice phases VII and X driven by monopole screening (2026), unpublished preprint.

## SUPPLEMENTAL MATERIAL

### Dual Mapping to the $XY$ Model at Finite Temperatures

In the main text, we introduced the duality mapping to the classical  $XY$  model in the monopole-free limit ( $v = 0$ ). Here, we generalize this mapping to finite temperatures, where the local constraints are relaxed and thermal monopoles with local charge  $Q_{\mathbf{r}} = \nabla \cdot \mathbf{S}_{\mathbf{r}} \neq 0$  are thermally excited.

To enforce this generalized local constraint, we introduce a continuous phase field  $\theta_{\mathbf{r}} \in [0, 2\pi)$  at each diamond-lattice site  $\mathbf{r}$  via the Fourier integral representation of the Kronecker delta:

$$\delta_{\nabla \cdot \mathbf{S}_{\mathbf{r}}, Q_{\mathbf{r}}} = \int_0^{2\pi} \frac{d\theta_{\mathbf{r}}}{2\pi} e^{-i\theta_{\mathbf{r}} \nabla \cdot \mathbf{S}_{\mathbf{r}} + i\theta_{\mathbf{r}} Q_{\mathbf{r}}}. \quad (14)$$

By inserting this integral into the partition function  $Z$  and performing a discrete integration by parts on the lattice,  $\sum_{\mathbf{r}} \theta_{\mathbf{r}} \nabla \cdot \mathbf{S}_{\mathbf{r}} = -\sum_{\ell} \nabla \theta_{\ell} S_{\ell}^z$  (where  $\nabla \theta_{\ell} := \theta_{\mathbf{r}_B} - \theta_{\mathbf{r}_A}$ ), we find that the spin and monopole degrees of freedom decouple. The partition function thus factorizes into link-dependent and site-dependent terms:

$$\begin{aligned} Z &= \sum_{\{Q_{\mathbf{r}}\}} \sum_{\{S_{\ell}^z\}} \prod_{\mathbf{r}} \left( \int_0^{2\pi} \frac{d\theta_{\mathbf{r}}}{2\pi} e^{-i\theta_{\mathbf{r}} \nabla \cdot \mathbf{S}_{\mathbf{r}} + i\theta_{\mathbf{r}} Q_{\mathbf{r}}} \right) v^{\sum_{\mathbf{r}} Q_{\mathbf{r}}^2} w^{\sum_{\ell} (S_{\ell}^z)^2} \\ &= \int \mathcal{D}\theta \prod_{\ell} \left( \sum_{S_{\ell}^z \in \{0, \pm 1\}} e^{iS_{\ell}^z \nabla \theta_{\ell}} w^{(S_{\ell}^z)^2} \right) \prod_{\mathbf{r}} \left( \sum_{Q_{\mathbf{r}}} v^{Q_{\mathbf{r}}^2} e^{iQ_{\mathbf{r}} \theta_{\mathbf{r}}} \right) \\ &= \int \mathcal{D}\theta \prod_{\langle \mathbf{r}, \mathbf{r}' \rangle} [1 + 2w \cos(\theta_{\mathbf{r}} - \theta_{\mathbf{r}'})] \prod_{\mathbf{r}} \left[ 1 + 2 \sum_{Q_{\mathbf{r}} > 0} v^{Q_{\mathbf{r}}^2} \cos(Q_{\mathbf{r}} \theta_{\mathbf{r}}) \right], \end{aligned} \quad (15)$$

where  $\mathcal{D}\theta := \prod_{\mathbf{r}} \frac{d\theta_{\mathbf{r}}}{2\pi}$  is the integration measure. Note that  $Q_{\mathbf{r}}$  takes integer values ranging from  $-4$  to  $4$ , representing the discrete divergence of four spins at a site.

In the low-temperature regime ( $w \ll 1$  and  $v \ll 1$ ), we employ the Taylor expansion  $\ln(1 + X) \approx X$ . Since the statistical weight scales as  $v^{Q_{\mathbf{r}}^2}$ , the summation is dominated by the fundamental monopole excitations ( $Q_{\mathbf{r}} = \pm 1$ ). Neglecting higher-order terms, the partition function converges to the effective action:

$$Z \approx \int \mathcal{D}\theta \exp \left[ 2w \sum_{\langle \mathbf{r}, \mathbf{r}' \rangle} \cos(\theta_{\mathbf{r}} - \theta_{\mathbf{r}'}) + 2v \sum_{\mathbf{r}} \cos \theta_{\mathbf{r}} \right]. \quad (16)$$

This result confirms that the thermal monopoles manifest as a uniform external magnetic field (a sine-Gordon potential) coupled to the emergent  $XY$  phase variables.

### Mapping to the Ising Model with a Magnetic Field

To investigate the effects of thermal monopoles ( $v > 0$ ) in the large- $w$  regime, we generalize Pauling's approximation to configurations with nonzero monopole charges and establish a term-by-term correspondence with the high-temperature expansion of the 3D Ising model in a magnetic field.

At finite temperatures, thermal monopoles geometrically act as endpoints of the defect strings. The partition function can be expressed as a sum over general graph configurations  $G$  that may contain endpoints and self-intersections:

$$Z = w^{2N} \sum_G \left( \frac{1}{w} \right)^{|G|} W_v(G), \quad (17)$$

where  $W_v(G)$  is the weighted number of valid background spin configurations for a fixed graph  $G$ , defined by

$$W_v(G) := \sum_{\{Q_{\mathbf{r}}\}} \sum_{\{S_{\ell}^z\}} \left( \prod_{\mathbf{r}} \delta_{\nabla \cdot \mathbf{S}_{\mathbf{r}}, Q_{\mathbf{r}}} \right) \left( \prod_{\ell \in G} \delta_{S_{\ell}^z, 0} \right) \left( \prod_{\ell \notin G} \delta_{|S_{\ell}^z|, 1} \right) v^{\sum_{\mathbf{r}} Q_{\mathbf{r}}^2}. \quad (18)$$

Let  $d_0(\mathbf{r})$  be the number of defect links (fixed to  $S_\ell^z = 0$ ) connected to a given site  $\mathbf{r}$ . The remaining  $4 - d_0(\mathbf{r})$  links can freely take  $\pm 1$ . We define the local state sum  $z(d_0)$  by summing the statistical weight  $v^{Q^2}$  over all  $2^{4-d_0}$  possible assignments:

$$z(d_0) := \sum_Q \binom{4-d_0}{\frac{4-d_0+Q}{2}} v^{Q^2}. \quad (19)$$

In the low-temperature regime ( $v \ll 1$ ), we neglect higher-order monopole contributions (e.g.,  $v^4$ ). The local state sums are evaluated as:

$$\begin{aligned} d_0 = 0: & \quad Q = 0 \text{ dominates, giving } z(0) \approx \binom{4}{2} v^0 = 6. \\ d_0 = 1: & \quad Q = \pm 1, \text{ giving } z(1) \approx 2 \binom{3}{1} v = 6v. \\ d_0 = 2: & \quad Q = 0 \text{ dominates, giving } z(2) \approx \binom{2}{1} v^0 = 2. \\ d_0 = 3: & \quad Q = \pm 1, \text{ giving } z(3) \approx 2 \binom{1}{0} v = 2v. \\ d_0 = 4: & \quad Q = 0, \text{ giving } z(4) = \binom{0}{0} v^0 = 1. \end{aligned} \quad (20)$$

Under Pauling's approximation, the total weight  $W_v(G)$  is estimated by multiplying the  $2^{2N-|G|}$  completely free degrees of freedom by the probabilities  $z(d_0)/2^{4-d_0}$  for realizing the specific charge configurations at all sites:

$$W_v(G) \approx 2^{2N-|G|} \prod_{\mathbf{r}} \frac{z(d_0(\mathbf{r}))}{2^{4-d_0(\mathbf{r})}} = 2^{|G|-2N} \prod_{\mathbf{r}} z(d_0(\mathbf{r})), \quad (21)$$

where we used the identity  $\sum_{\mathbf{r}} [4 - d_0(\mathbf{r})] = 4N - 2|G|$ . Let  $V_k$  denote the number of sites in graph  $G$  with degree  $k$  (i.e.,  $d_0(\mathbf{r}) = k$ ). The product over sites becomes  $z(0)^{V_0} z(1)^{V_1} z(2)^{V_2} z(3)^{V_3} z(4)^{V_4}$ . Factoring out the vacuum weight  $W(\emptyset) \approx 2^{-2N} z(0)^N$  and using  $V_0 = N - V_1 - V_2 - V_3 - V_4$ , we obtain

$$\begin{aligned} W_v(G) & \approx W(\emptyset) 2^{|G|} \left( \frac{z(1)}{z(0)} \right)^{V_1} \left( \frac{z(2)}{z(0)} \right)^{V_2} \left( \frac{z(3)}{z(0)} \right)^{V_3} \left( \frac{z(4)}{z(0)} \right)^{V_4} \\ & = W(\emptyset) 2^{|G|} v^{V_1} \left( \frac{1}{3} \right)^{V_2} \left( \frac{v}{3} \right)^{V_3} \left( \frac{1}{6} \right)^{V_4}. \end{aligned} \quad (22)$$

We eliminate  $V_2$  by exploiting the graph-theoretic identity for the sum of degrees:  $V_1 + 2V_2 + 3V_3 + 4V_4 = 2|G| \implies V_2 = |G| - \frac{1}{2}V_1 - \frac{3}{2}V_3 - 2V_4$ . This yields

$$\begin{aligned} W_v(G) & \approx W(\emptyset) 2^{|G|} v^{V_1} \left[ \left( \frac{1}{3} \right)^{|G|} (\sqrt{3})^{V_1} (3\sqrt{3})^{V_3} 9^{V_4} \right] \left( \frac{v}{3} \right)^{V_3} \left( \frac{1}{6} \right)^{V_4} \\ & = W(\emptyset) \left( \frac{2}{3} \right)^{|G|} (\sqrt{3}v)^{V_1+V_3} \left( \frac{3}{2} \right)^{V_4}. \end{aligned} \quad (23)$$

The sum of odd-degree vertices  $V_1 + V_3$  corresponds to the total number of endpoints  $|\partial G|$  in the graph. Assuming a dilute gas where self-intersections ( $V_4$ ) are rare, we approximate  $(3/2)^{V_4} \approx 1$ . The partition function then simplifies to

$$Z \approx w^{2N} W(\emptyset) \sum_G \left( \frac{2}{3w} \right)^{|G|} (\sqrt{3}v)^{|\partial G|}. \quad (24)$$

We compare this result with the high-temperature expansion of the 3D Ising model in a uniform external magnetic field  $h$ , defined as  $Z_{\text{Ising}} = \sum_{\{\sigma_{\mathbf{r}}\}} \exp \left( K \sum_{\langle \mathbf{r}, \mathbf{r}' \rangle} \sigma_{\mathbf{r}} \sigma_{\mathbf{r}'} + h \sum_{\mathbf{r}} \sigma_{\mathbf{r}} \right)$ . The expansion yields

$$Z_{\text{Ising}} = (\cosh K)^{2N} (\cosh h)^N 2^N \sum_G x^{|G|} y^{|\partial G|}. \quad (25)$$

This establishes a mapping between the microscopic physical parameters and the effective Ising parameters:

$$x := \tanh K = \frac{2}{3w}, \quad (26)$$

$$y := \tanh h = \sqrt{3}v. \quad (27)$$